Synthesis and Electrochemistry of Free-Base Porphyrins Bearing Trifluoromethyl meso-Substituents

Shaymaa Al Shehimy, Denis Frath, Elise Dumont, Floris Chevallier, Christophe Bucher

Synthesis and Electrochemistry of Free-Base Porphyrins Bearing Trifluoromethyl meso-Substituents

Shaymaa Al Shehimy, Denis Frath, Elise Dumont, Floris Chevallier* and Christophe Bucher*[a]

[a] Ms. S. Al Shehimy, Dr. D. Frath, E, Pr. E. Dumont, Dr. F. Chevallier and Dr. C. Bucher
Laboratoire de Chimie ; Université de Lyon, École Normale Supérieure de Lyon, CNRS UMR 5182 ; 46 allée d'Italie, F-69364 Lyon, France
E-mail: floris.chevallier@ens-lyon.fr; christophe.bucher@ens-lyon.fr

Supporting information for this article is given via a link at the end of the document.

Abstract: CF_3-substituted porphyrins have attracted increasing interest over the past decade. However, the number of examples reported in the literature remains quite limited and much remains to be done to understand the properties and reactivity of these molecules. We are now reporting on the synthesis of a series of free base porphins incorporating one, two and three CF_3 substituents, including the 5,10,15-tris(CF_3) substituted porphyrin which has never been described before. We have also carried out detailed electrochemical and spectroscopic analyses aiming at assessing the EWG properties of the CF_3 substituents compared to the widely used C_6F_5. Our studies led us to propose an interpretation of the quite unusual electrochemical signature of these molecules featuring three successive one-electron reduction waves.

Introduction

The chemistry of porphyrins has been in continuous development ever since the discovery of hematoporphyrin by Nencki and Zeleski in the 1900s.[1] The key role of the *meso*- and/or β-substituents on the spectroscopic, chemical, photophysical and electronic properties of these aromatic macrocycles has led researchers to conceive a whole range of peripheral modification strategies. Much efforts have focused over the past decades at providing access to peripherally crowded macrocycles,[2] at introducing water-solubilizing groups,[3] at expanding π-conjugation or at introducing peripheral coordination sites.[4] These essential works have paved the way for applications in many different fields such as in catalysis, sensing, medicine and in energy related domains.[5, 6] The introduction of electron-withdrawing groups (EWG) have proved particularly useful to enhance the axial binding ability of metalloporphyrins,[7] to tune the redox activity of porphyrins and of the metal ion inserted in their cavities[8, 9] or to enable the synthesis/stabilization of particular porphyrin analogs.[10, 11] Such modifications are thus of paramount importance for synthetic purposes and to promote the applications of porphyrins in (electro)catalysis,[12] sensing[13] or in molecular magnetism.[14]

The most widely used electron-withdrawing substituent in porphyrin chemistry so far is the pentafluorophenyl group. The latter is easily introduced at the *meso* positions of porphyrins using acid-catalyzed Rothemund-Lindsey type of condensations[15] between selected pyrrole derivatives and the commercially available 2,3,4,5,6-pentafluorobenzaldehyde. The large gain in popularity of this substituent over the past decades is due the availability of this key reactant, to the presence of five strongly electronegative fluorine atoms and also to the chemical reactivity of the para fluorine atom which can be exploited for further functionalization. It should be noted however that other substituents, like the 4-trifluoromethylphenyl, 3,5-bis(trifluoromethyl)phenyl,[16, 17] nitro,[18] cyano, halogens, 4-nitrophenyl or 4-pyridiunium, have also been used, albeit to a lesser extent, to tune the electron density of porphyrins.[19] In addition to their EWG character, fluorine atoms are also particularly interesting for medicinal applications.[20] The incorporation of fluorine atoms is for instance known to enhance the pharmacological activity of organic molecules[21] while ^{19}F-NMR spectroscopy may also prove extremely useful as a monitoring tool in biological media.

The CF_3 substituents is a particularly interesting/powerful EWG which has already been introduced at the β-position of porphyrins. These syntheses require the introduction of CF_3 groups prior to pyrrole formation[22, 23] or the use of halogenated porphyrin-based intermediates.[24-28] These substituents have also been introduced at the *meso* positions in corroles[29-31] and expanded porphyrins.[32] It also includes a handful of articles reporting on the synthesis of mono,[33] bis-(5,15)[34-38] and tetra-substituted[12, 35, 39-43] porphyrin derivatives. All these products have been obtained either from reactions between trifluoroacetaldehyde and pyrrole [44] or using a CF_3-substituted dippyromethane as an intermediate.[45, 46]

We are now reporting on the synthesis of a series of free base *meso*-substituted porphyrins incorporating one, two and three CF_3 substituents, including the 5,10,15- tris(CF_3) substituted porphyrin which has never been reported before. We have also carried out detailed electrochemical and spectroscopic analyses aiming at assessing the EWG properties of the CF_3 substituents compared to the widely used C_6F_5.

Results and Discussion

Synthesis

Our strategy to synthesize the targeted molecules was inspired by the work of Lindsey and co-workers on porphyrins bearing different *meso*-substituents.[15] The targeted free base macrocycles bearing electron-withdrawing substituents were prepared using a rational methodology involving acylation at the 1,9-positions of the trifluoromethyl-substituted dipyrromethane **1**, followed by condensation with a dipyrromethane to give the corresponding *trans*-A_2B_2-porphyrin **5**H_2, and A_3B-porphyrins **4**H_2 and **6**H_2 (Scheme 1).[47] For this purpose, the 5-trifluoromethyldipyrromethane (**1**) was isolated in a moderate yield by condensation of pyrrole and trifluoroacetaldehyde, used as its hemiacetal, in the presence of stoichiometric amounts of trifluoroacetic acid. [29] Treatment of **1** with trifluoroacetic anhydride at ambient temperature afforded the targeted 1,9-bis(trifluoroacetyl) derivative **2** in 98% yield.[32] Standard

formylation of **1** with two equivalents of Vilsmeier reagents ($POCl_3$/DMF) then afforded the key intermediate **3** in 67% yield.[48]

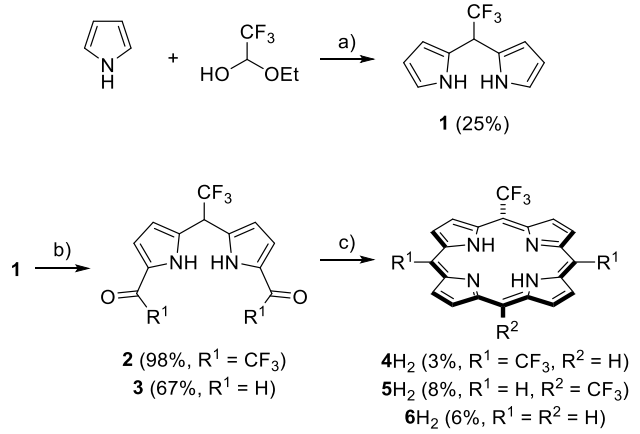

Scheme 1. For **1**: a) TFA, CH_2Cl_2, RT, 12 h. For 2: b) $(CF_3CO)_2O$, toluene, RT, 5 h. For **3**: b) $POCl_3$, DMF, 0°C, 1.5 h. For 4: c) $NaBH_4$, then 2,2'-dipyrrolylmethane, MsOH, CH_2Cl_2, 35 °C, 1.5 h, then DDQ. For **5**H_2: c) $NaBH_4$, then 1, $Yb(OTf)_3$, CH_2Cl_2, 35 °C, 1.5 h, then DDQ. For **6**H_2: c) $NaBH_4$, then 2,2'-dipyrrolylmethane, MsOH, CH_2Cl_2, 35 °C, 1.5 h, then DDQ.

In this study, we also focused on *meso*-pentafluorophenyl-substituted porphyrins as reference compounds. The *bis* (**7**H_2), *tris* (**8**H_2) and *tetra* (**9**H_2) C_6F_5-substituted porphyrin derivatives were obtained using methods described in the literature (Scheme 2).[49, 50]

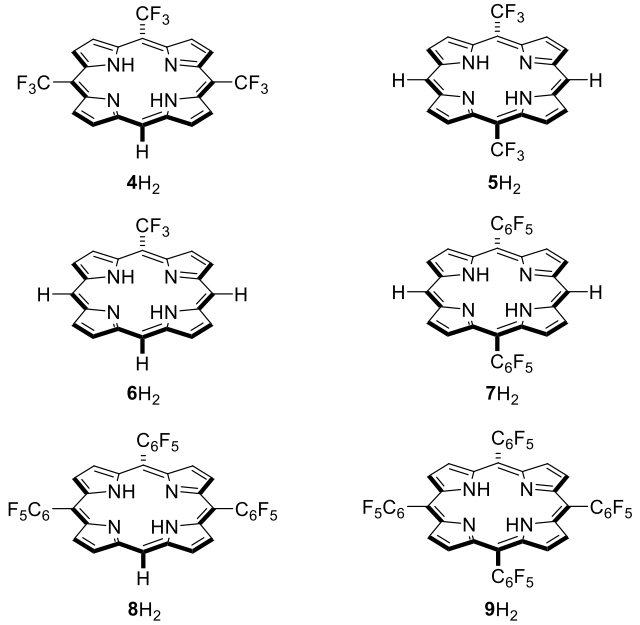

Scheme 2. CF_3- (**4**-**6**H_2) and C_6F_5-substituted (**7**-**9**H_2) porphyrins investigated in this study.

The targeted trifluoromethyl *meso*-substituted porphyrins **4**H_2-**6**H_2 were fully characterized by ^{1}H-NMR spectroscopy using 1D- and 2D-NMR experiments. The number and relative intensities of the signals observed in the ^{1}H- and ^{19}F-NMR spectra recorded in deuterated chloroform (1mM) at room temperature are in agreement with the proposed structures. Observation of one or two ^{19}F signals in the spectrum of **4**H_2 and **5**H_2 is for instance fully consistent with the symmetry of these molecules leading to the chemical equivalence of both CF_3 substituents introduced at position 5 and 15 of the porphyrin ring (Figure 1). Detailed attribution of the ^{1}H signals are shown in Figure 1. As expected, the electron-withdrawing character of the trifluoromethyl groups is brought to light through the chemical shift window, which shortens with the number of CF_3 groups. This trend reflects a weakening of the aromatic ring current due to a decrease of the electron density on the porphyrin ring. The effect is particularly strong on the signals attributed to the inner NH resonances shifting from -3.39 to -2.71 ppm upon introducing one and three CF_3 substituents, respectively. This effect is far less marked in the aromatic region involving resonances attributed to the β and meso-hydrogen atoms. The maximum shift is observed for the *meso* hydrogen atoms undergoing a 0.12 ppm upfield shift between **4**H_2 and **6**H_2. The limited shift of the aromatic signals can actually be explained by the fact that these protons are subjected to two opposite effects: a weakening of the aromatic ring current leading to an upfield shift of the signals attributed to all protons located outside the ring and the EWG effect of the CF_3 substituents leading to a downfield shift of the same signals.

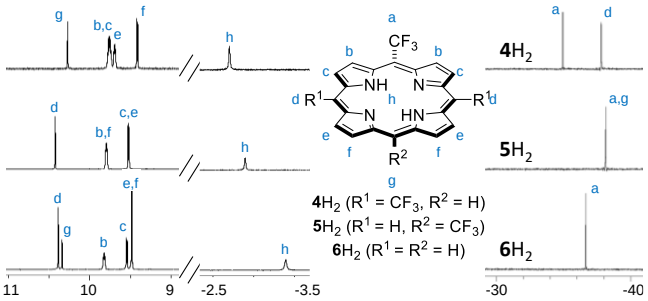

Figure 1. Partial ^{1}H- (left) and ^{19}F- (right) NMR spectra of **4**H_2, **5**H_2 and **6**H_2 (1 mM, $CDCl_3$, 25 °C, 400 MHz).

These compounds were further characterized by UV-Vis absorption spectroscopy. The spectra of **4**H_2-**6**H_2 recorded in acetone exhibit one intense Soret band centered at λ_{max} = 391-398 nm (8.3 10^3 - 25 10^3 $M^{-1}.mm^{-1}$) and four much weaker Q bands, including shoulders (See Fig ESI15). The absence of aggregation in these conditions was revealed by the linear evolution of the intensity measured at λ_{max} as a function of concentration (see Fig SI6). As expected, the addition of CF_3 substituents on the porphyrin core leads to significant bathochromic shifts of the absorption bands and to a decrease of the molar extinction coefficients from 18 10^3 $M^{-1}.mm^{-1}$ for **6**H_2 down to 8.9 10^3 $M^{-1}.mm^{-1}$ for **4**H_2 (see Table 1). We found however no clear linear dependence of the max wavelengths with the number of CF_3 substituents. Increasing the number of CF_3 has also a much stronger effect on the Q bands than on the Soret band which undergoes only a 7nm shift by increasing the number of CF_3 from 1 to 3 (**4**H_2 to **6**H_2)

Taken together, the spectroscopic data discussed above are consistent with the conclusion that the introduction of CF_3 substituent lead to weakening of the electron density and of the aromaticity of the porphyrin ring. DFT investigations carried out on **4**H_2, **5**H_2 and **6**H_2 moreover revealed that the addition of 1, 2 or 3 CF_3 groups does not induce significant distortion of the porphyrin plane, which support the conclusion that all the shifts discussed above only result from the electronegative character of the CF_3 substituents.

Table 1. Maximum wavelength (λ_{max} in nm) and extinction coefficient values (ε in $M^{-1}\,mm^{-1}$) measured for **4**H_2, **5**H_2 and **6**H_2 in acetone and dichloromethane.

		Soret Band		Q1		Q2		Q3		Q4	
		λ_{max}	ε	λ_{max}	ε	λ_{max}	ε	λ_{max}	ε	λ_{max}	ε
Acetone	**6**H_2	391	18200	492	1100	523	820	564	480	617	560
	5H_2	390	8300	498	480	533	840	573	260	626	750
	4H_2	398	8900	504	660	538	630	583	330	636	610
DCM	**6**H_2	394	9500	494	470	528	240	567	130	619	90
	5H_2	393	13400	498	660	536	1180	577	290	628	1030
	4H_2	402	19700	505	1180	538	1060	587	410	637	1090

The EWG effect of the CF_3 groups was further studied upon assessing the ability of the inner nitrogen atoms to accept or release protons in the presence of added acid and base, respectively.

The protonation of porphyrins was studied in dichloromethane upon recording changes in the Soret and Q bands intensities and maximum wavelengths in the presence of trifluoroacetic acid (TFA). Initial attempts revealed that neither **4**H_2, **5**H_2 nor **6**H_2 can be protonated in DMF, which is consistent with the expected weak basicity of the inner nitrogens. However, protonation of those core N-atoms was eventually achieved in dichloromethane. The experimental data collected in these conditions in the presence of TFA are moreover in agreement with the direct formation of the doubly protonated species $[\mathbf{P}H_4]^{2+}$ from **P**H_2 with no evidence of the monoprotonated intermediate $[\mathbf{P}H_3]^{+}$, as revealed by the observation of a clear isosbestic point in the titration curves and by the development of a single set of signals (Soret and Q bands). The spectroscopic data collected upon addition of TFA to a solution of **4**H_2 are shown in Figure 2A as an illustration of such behavior. Similar data collected with **5**H_2 and **6**H_2 are shown in the ESI section (Figure ESI17A/C). Protonation systematically led to bathochromic and hyperchromic shifts of the Soret band and to the development of only two Q bands. Most importantly, we found that the amount of TFA required to produce the bisprotonated porphyrins $[\mathbf{P}H_4]^{2+}$ from **P**H_2 increase with the number of CF_3 substituents (see Figure 2C) as a result of the decrease in the basicity of the inner nitrogens.

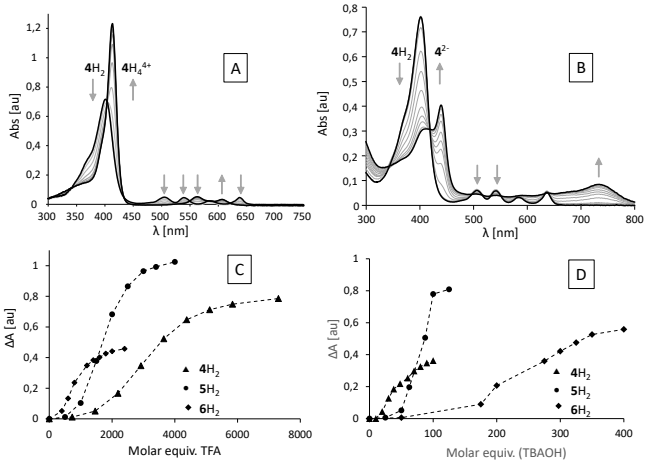

Figure 2. Variation of the UV/Vis absorption spectra upon titration of (A) $5.87x10^{-6}$ M DCM solution of **4**H_2 with TFA and (B) $9.04x10^{-6}$ M DMF solution of **4**H_2 with 0,1 M solution of TBAOH in MeOH/Toluene (1cm optical path). Variation of ΔA versus (C) molar equiv. of TFA and (D) molar equiv. of TBAOH during the acid and base titration of **4**H_2-**6**H_2 in DCM and DMF, respectively.

Accordingly, we found that the acidity of the inner NH's increase with the number of CF_3 groups. This was easily revealed upon recording changes in the Soret and Q bands intensities and maximum wavelengths in the presence of tetra-*n*-butylammonium hydroxide (TBAOH). Here again, as illustrated in Figure 2B with the curves recorded with **4**H_2, all the experimental data collected in these conditions are consistent with the direct formation of the dianionic species $\mathbf{P}^{2-}$ from **P**H_2. The formation of $\mathbf{4}^{2-}$ is revealed in in Figure 2B through the decrease in the intensity of the Soret and Q bands attributed to **4**H_2 at the expense of new signals developing at 439 nm and 734 nm.

Electrochemical studies

The electrochemical properties of the CF_3-substituted porphyrins **4**H_2, **5**H_2 and **6**H_2 were investigated in DMF in the presence of tetra-*n*-butylammonium hexafluorophosphate used as electrolyte. For comparison purposes, similar analyses were conducted on the reference compounds **7**H_2, **8**H_2 and **9**H_2, incorporating C_6F_5 substituents.

The CV curves recorded for **4**H_2, **5**H_2 and **6**H_2 display similar features including three successive one-electron reductions and one oxidation centered on the porphyrin ring. Detailed electrochemical data are collected in Table 2 but only the CV curves recorded with the 5,10,15-substituted compounds **4**H_2 and **8**H_2 are shown in Figure 3. CV curves recorded for **5**H_2 and **6**H_2 are provided in the ESI section (Figure ESI 1 & 2). The relative number of electrons involved in each wave was assessed from electrolysis and measurements recorded in steady state conditions at rotating disc electrodes (dashed lines in Figure 3). It should also be mentioned that similar CVs were obtained when using dichloroethane as the solvent (see Fig ESI 3).

On the anodic side, only one fully irreversible oxidation wave is observed in the accessible potential domain. Such irreversibility, frequently observed for free base porphyrins, is usually attributed to the formation of unstable cation radicals $\mathbf{P}H_2^{+\bullet}$ readily reacting with traces of nucleophiles attacking at one of the meso position to afford isoporphyrins. RDE measurements carried out on the whole accessible potential window revealed that the intensity of the oxidation waves is significantly larger, nearly double, than that of the first reduction wave, which support the conclusion that the oxidation product is easier to oxidize than the starting porphyrin.

In agreement with the proposed attribution of the first oxidation and reduction waves to porphyrin-centered processes yielding $PH_2^{+\bullet}$ and $PH_2^{\bullet-}$, we found a similar calculated HOMO-LUMO gap (~2.1 V) for **4**H_2, **5**H_2 and **6**H_2 (Table 2)**.** The EWG character of the CF_3 substituents was then assessed from the E^{1c} and E^{1a} values collected for the CF_3 and C_6F_5-substituted compounds **4**H_2-**9**H_2**.** The effect of the EWG can be seen on the CV curves depicted in Figure 4A showing the shift of the first oxidation and

reduction waves with the number of substituents. These data bring to light the much larger EWG character of the CF_3 substituent compared to the C_6F_5. They are also consistent with the conclusion that two CF_3 substituents have stronger EWG effects than four C_6F_5 substituents. We also studied the way the oxidation and reduction potentials shifts with the number of substituents and compared the EWG character of CF_3 versus C_6F_5. Such comparison can be easily achieved from the electrochemical data collected in Table 1, upon taking advantage of the known dependence of electrochemical signature of porphyrins with the Hammett constants of the substituents introduced at their *meso*-positions.[51, 52]

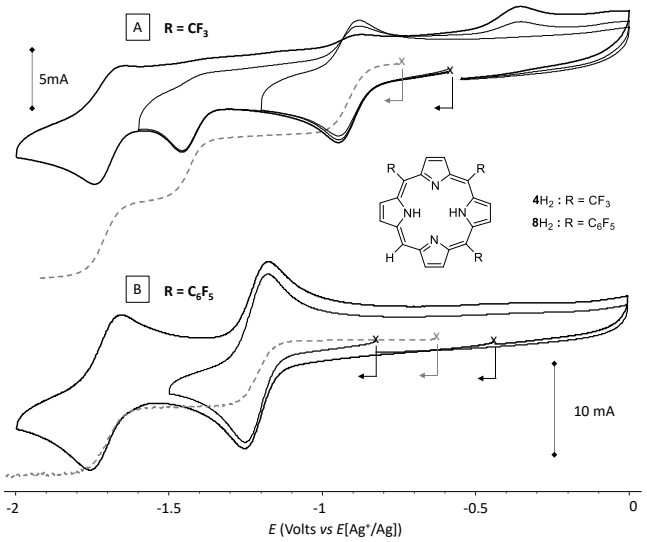

Figure 3. Voltamperometric curves of DMF solutions of **4**H_2 and **8**H_2 ($1x10^{-3}$ M + 0.1M in TBAPF6) recorded at a vitreous carbon working electrode (full line, Ø = 3 mm, 0.1 $V.s^{-1}$) and at a rotating disk electrode(dashed lines, Ø = 3 mm, 0.01 $V.s^{-1}$, 500 $rd.min^{-1}$).

In all cases studied, the stability of the anion radical state **4**$H_2^{\bullet-}$ and $8H_2^{\bullet-}$ at the CV time scale was revealed by the reversibility of the first one-electron reduction wave observed above -1.5 V (see in Table 2 and Fig ESI4, ΔE_P = 60 to 65 mV at 100mV.s^{-1}, $I_p=\alpha(v)^{1/2}$). The exact attribution of the two subsequent reductions of **4**$H_2^{\bullet-}$ at E^{2c} and E^{3c} proved more difficult, mainly due to the observation of three reduction waves in the whole accessible potential domain, which stands in sharp contrast with the standard electrochemical signature of porphyrins involving only two successive reduction yielding the anion radical (**P**$H_2^{\bullet-}$) and dianion (**P**H_2^{2-}) species, respectively.[53-58] Such standard signature was for instance observed with the C_6F_5-substituted reference compounds **7**H_2, **8**H_2 and **9**H_2, which contrasts with the three reduction waves observed with the CF_3-subsituted compounds **4**H_2, **5**H_2 and **6**H_2 (see Figure 3A). As a matter of facts, more than two reduction waves can be observed on the CV curves of porphyrins *i*) when electroactive substituents and/or metal centers are involved *ii*) with porphyrins incorporating very strong EWG substituents like NO_2 or CN or *iii*) when studying the electrochemistry of porphyrins in solvents featuring unusually large accessible potential windows.[59-62]

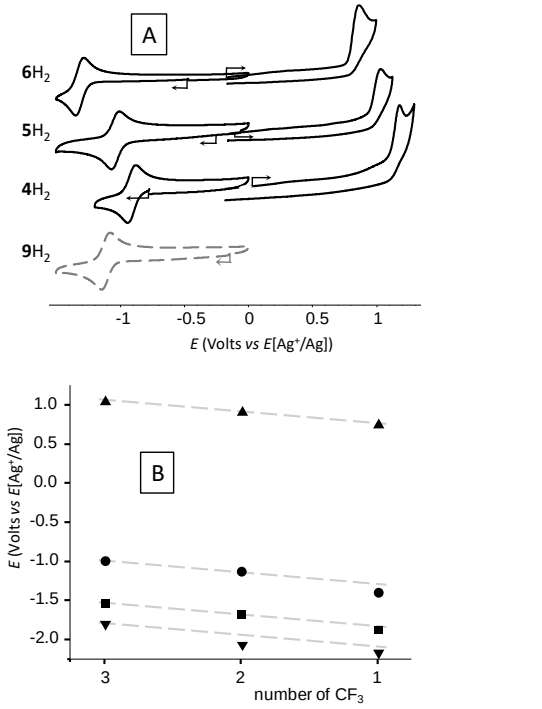

Figure 4. A) first reduction and first oxidation waves observed on the CV curved of DMF solution of **4**H_2, **5**H_2, **6**H_2 and **9**H_2 ($1x10^{-3}$M + 0.1M in $TBAPF_6$) recorded at a vitreous carbon working electrode (Ø =3 mm, *E* vs Ag^+/Ag (10^{-2} M), 0.1 $V.s^{-1}$). B) Plots of the oxidation and reduction potential values recorded for **4**H_2, **5**H_2 and **6**H_2 (E^{1a}, E^{1c}, E^{2c}, E^{3c}, see table 1) as a function of the number of CF_3 substituents.

As shown in table 1, the second reduction of **4**H_2, **5**H_2 and **6**H_2 was systematically observed as a fully irreversible wave shifted ~500 mV below the first one. Those reduction waves involving formation of the dianions PH_2^{2-} remained irreversible at all investigated scan rates (0.1-1V/s) and their relative intensity was found to remain the same regardless of the number of CF_3 substituents on the porphyrin ring (see Figure ESI 7). Previous reports by Kadish and coworkers recently established the ability of porphyrins bearing extremely strong EWG groups to undergo up to four consecutive reduction processes yielding stable trianions radicals $PH_2^{\bullet3-}$ and even tetraanions PH_2^{4-}.[60] For all these compounds however, the potential shift measured between the first and the second reduction waves were consistently found to be much greater (nearly double) than that measured between the second and third reductions of **4**H_2, **5**H_2 and **6**H_2 (E^{2c} and E^{3c} in Table 2). The plots shown in Figure 4B also reveal that the potential values associated to the observed oxidation and reduction processes E^{1a}, E^{1c}, E^{2c} and E^{3c} decrease with similar slopes as a function of the number of CF_3 substituents. All these findings thus support the conclusion that all the observed reduction processes are centered on the porphyrin ring and that the first reduction wave (E^{1c} in in Table 2) yields a stable porphyrin-based anion radical **P**$H_2^{\bullet-}$ which is then submitted to a second one-electron reduction (E^{2c} in in Table 2) affording an unstable dianion **P**H_2^{2-}. This latter compound is then transformed at the CV timescale via a coupled chemical step into a new species being reduced at E^{3c} (in Table 2).

Table 2. Potential values (Volt) measured by cyclic voltammetry for **4**H_2-**9**H_2 in DMF. The number of electrons transferred and the peak-to-peak potential for each electrochemical process is shown between parentheses.

	E^{3c} (n, ΔE_P) $P^{2-}/P^{\bullet 3-}$	E^{2c} (n, ΔE_P) $P^{\bullet -}/P^{2-}$	E^{1c} (n, ΔE_P) $P/P^{\bullet -}$	E^{1a} $P/P^{\bullet +}$	H-L gap
4H_2	-1.79 [a] (1e-, na)	-1.522 [a]	-0.984 [b] (1e-, 66)	1.062 [a]	2.047
5H_2	-2.06 [a] (1e-, na)	-1.670 [a]	-1.116 [b] (1e-, 63)	0.93 [a]	2.045
6H_2	-2.16 [a] (1e-, na)	-1.861 [a]	-1.389 [b] (1e-, 60)	0.762 [a]	2.151
7H_2	-	-1.979 [a]	-1.375 [b] (1e-, 74)	0.872 [a]	2.247
8H_2	-	1.785 [b] (1e-, 131)	-1.286 [b] (1e-, 73)	0.992 [a]	2.278
9H_2	-	-1.674 [b] (1e-, 74)	-1.187 [b] (1e-, 65)	1.085 [a]	2.271

[a] *Peak potential; irreversible redox wave (V)*
[b] *Half-wave potential (V)*
ΔE_p: Peak to peak potential difference (mV)
Potential values (V) are referenced versus the Fc^+/Fc couple

Further investigation mostly aimed at identifying the chemical steps coupled to the formation of the dianion PH_2^{2-}. The electrochemical reduction of organic molecules is particularly well known to produce basic species capable of abstracting protons from their environment, as observed with numerous aromatic hydrocarbons and heterocyclic compounds including porphyrins,[63-66] or to release H_2, as suggested to occur upon reduction of various nitro-substituted organic molecules or porphyrins.[65, 67, 68]

First studies aimed at studying the electrochemical response of **4**H_2, **5**H_2 and **6**H_2 in the presence of added base or acid. As can be seen in the CV curves shown in Figure 5, addition of increasing amounts of TBAOH led to the disappearance of the first and second reduction waves attributed to the successive formation of $\mathbf{P}H_2^{\bullet -}$ and $\mathbf{P}H_2^{2-}$. The CV curves recorded after addition of an excess TBAOH, yielding the fully deprotonated species P^{2-} (dashed lines in Figure 5A/B), displays one single reduction wave observed at the same potential as the third reduction wave of **P**H_2 (full line in Figure 5A/B). This behavior thus suggest that the chemical step coupled to the formation of $\mathbf{P}H_2^{2-}$ leads to the formation of the fully deprotonated species $\mathbf{P}^{2-}$. The mechanism proposed on the basis of these observations and of previous studies carried out on porphyrins[65] is detailed in Scheme 3.

The two first steps are the two consecutive one-electron reduction (Eq.1-2) yielding the unstable dianion $\mathbf{P}H_2^{2-}$ which evolves at the CV time scale into $\mathbf{P}^{2-}$ with concomitant release of H_2 (eq. 3).The overall process is thus a two electron reduction yielding $\mathbf{P}^{2-}$ and H_2 (eq.4).

Similar investigations were carried out using TFA as a proton source. Addition of TFA systematically led to a loss of the reversible character of the first reduction wave coming along with a two-fold increase in the peak current intensity, which suggests that the number of electrons transferred has doubled. This behavior is illustrated in Figure 6 with the diffusion-limited current recorded at a rotating disk electrode before and after addition of 2 molar equivalents of TFA to a solution of **4**H_2. We also found that further addition of acid led to a progressive shift of the first reduction wave towards less negative values but without changing its relative intensity. This fully irreversible reduction is also associated to an irreversible re-oxidation wave observed on the reverse scan at E_p ~ -0.2 V. The analysis of these data was carried out taking into account the acid-base experiments discussed above (see demonstrating that a full protonation of the weakly basic **P**H_2 species requires a large amount of TFA. The behavior observed in Figure 6 in the presence of little amount of TFA is thus attributed to a series of reduction and protonation steps consecutive to the formation of the more basic radical anion $\mathbf{P}H_2^{\bullet -}$ (eq. 1). According to the proposed mechanism shown in Scheme 3, the first coupled chemical process is the protonation of $\mathbf{P}H_2^{\bullet -}$ yielding $\mathbf{P}H_3^{\bullet}$ (eq. 3) which is readily reduced into $\mathbf{P}H_3^{-}$ and then further protonated to afford the neutral species **P**H_4 (eq. 3). Overall, the reduction wave observed after addition of TFA involves addition of two electrons and two protons to convert **P**H_2 into **P**H_4 (eq. 6). In agreement with the proposed reaction scheme, the irreversible oxidation wave observed at *ca* –0.2 V is thus attributed to the oxidation of this later species which can ultimately afford back the initial **P**H_2.

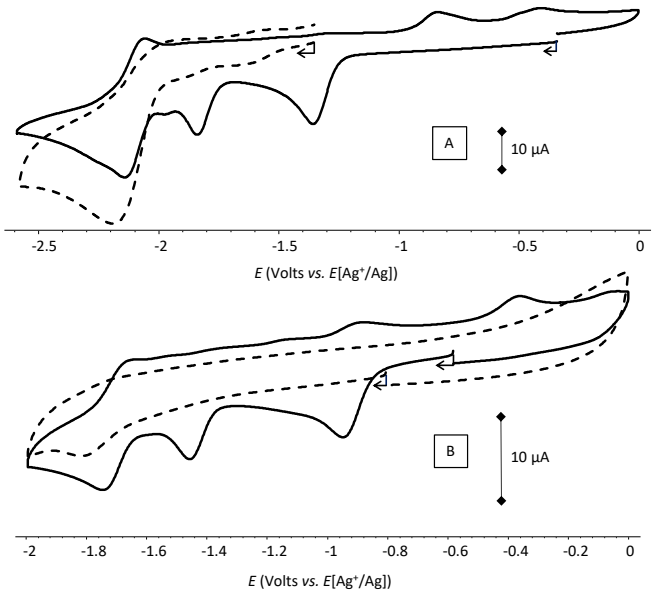

Figure 5. CV curves recorded before (full lines) and after addition (dashed line) of A) 8 or (B) 4 molar equivalents of tetra-n-butylammonium hydroxide (0.1 M in MeOH/Toluene) to 1 mM solutions of **6**H_2 and **4**H_2, respectively (GC WE ∅ 3mm, 100 $mV.s^{-1}$).

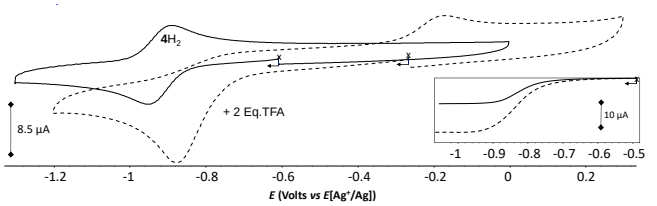

Figure 6. CV curves recorded before (full lines) and after addition (dashed line) of 2 molar equivalents of TFA (0.11 M in DMF) to a 0.945 mM solution of **4**H_2 (GC WE ∅ 3mm, 100 $mV.s^{-1}$).Inset : voltammperogram recorded in the same conditions at a rotating disk electrode (RDE, 10 $mV.s^{-1}$, 500 rd.min)

$$\mathbf{P}H_2 + e = \mathbf{P}H_2^{\bullet -} \quad (1)$$

$$\mathbf{P}H_2^{\bullet -} + e = \mathbf{P}H_2^{2-} \quad (2)$$

$$\mathbf{P}H_2^{2-} = \mathbf{P}^{2-} + H_2 \quad (3)$$

$$\mathbf{P}H_2 + 2e = \mathbf{P}^{2-} + H_2 \quad (4)$$

$$\mathbf{P}H_2 + e = \mathbf{P}H_2^{\bullet -} \quad (1)$$

$$\mathbf{P}H_2^{\bullet -} + H^+ = \mathbf{P}H_3^{\bullet} \quad (5)$$

$$\mathbf{P}H_3^{\bullet} + e = \mathbf{P}H_3^{-} \quad (6)$$

$$\mathbf{P}H_3^{-} + H^+ = \mathbf{P}H_4 \quad (7)$$

$$\mathbf{P}H_2 + 2e + 2H^+ = \mathbf{P}H_4 \quad (8)$$

Scheme 3. Proposed mechanisms

Spectroelectrochemistry

The stability and the spectroscopic signature of the reduced porphyrins was checked by spectro-electrochemistry (SEC) measurements carried out upon collecting time-resolved UV/Vis spectra during exhaustive reductions. The latter was carried out in a potentiostatic regime using a large surface platinum working electrode and a divided cell.

The SEC data collected with **4**H_2 are displayed in

These studies revealed that the addition of CF3 substituents on the porphyrin ring leads, as expected, to an increase in the energy gap between the neutral and radical anion species by ca. 0.2 eV per –CF3 moiety, and between the radical anion species and the dianion by 0.3-0.4 eV, which is easily explained by the fact the stabilization of the radical anions and of the dianions increases with the number of CF3 substituents. Key figures reported in the ESI section demonstrate that the stabilization associated to the first electron transfer ranges from -3.39 to -3.79 eV for the mono- and tri-substituted compounds, respectively, and that the second addition of electron is slightly less favorable ranging from -2.87 to -3.24 eV. The HOMO-LUMO energy gap is constant, close to 0.15 eV for the three systems independently of their number of CF3 substituents.

. Setting the electrode potential at E_{app} = -1.2 V led to the progressive disappearance of the initial Soret band centered at 394 nm at the expense of a less intense signal developing at λ_{max} =422 nm. Observation of a clean isosbestic point at 410 nm also confirms that no secondary reactions occur over the considered time range. The initial Q bands were also found to disappear at the expense of new bands developing in the visible and NIR range. The one electron reduced species **4**$H_2^{\bullet-}$ were found to be stable at the electrolysis time scale (~30 minutes). The latter species, produced by exhaustive electrochemical reduction at E_{app} = -1.2 V, was also identified by RDE measurements carried out after addition of one electrons/moles.

As expected from the CV data discussed above, further reduction of **4**$H_2^{\bullet-}$ at E_{app} = -1.53 V led to irreversible changes in the UV/Vis spectrum. The latter had little effects on the Soret Band but led to the disappearance of the signals at 626 and 814 nm at the expense of a broad absorption bands centered at 733 nm. The irreversible nature of the transformation associated to this second electron transfer was confirmed by failure to regenerate the initial porphyrin **4**H_2 by reoxydation. In support of the mechanism proposed in Scheme 3, we found that the broad band centered at 733 nm is similar to that observed upon formation of the deprotonated species **4**$^{2-}$.

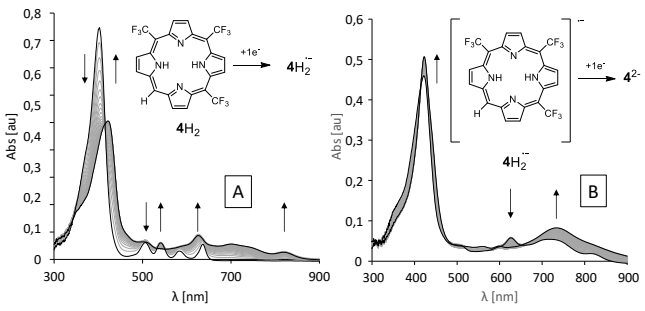

Figure 7. UV/vis spectra recorded during (A) the first (E_{app}= -1.2 V) and (B) the second (E_{app}= -1.53 V) exhaustive one-electron of **4**H_2 ($8.5x10^{-5}$ M) in DMF (0.1m $TBAPF_6$) (working electrode: Pt, 10 mL, l = 1 mm, t ≈ 30 min).

DFT calculations

The structures of **4**H_2-**6**H_2 were optimized by density functional theory (DFT) at the M062X/6-31+G(d,p) level of theory, using the self-consistent reaction field (SCRF) polarizable continuum model (PCM) to account for solvation in N,N-dimethylformamide. DFT calculations were performed using the Gaussian 16 Revision B.01 series of programs.

These studies revealed that the addition of CF_3 substituents on the porphyrin ring leads, as expected, to an increase in the energy gap between the neutral and radical anion species by ca. 0.2 eV per –CF_3 moiety, and between the radical anion species and the dianion by 0.3-0.4 eV, which is easily explained by the fact the stabilization of the radical anions and of the dianions increases with the number of CF_3 substituents. Key figures reported in the ESI section demonstrate that the stabilization associated to the first electron transfer ranges from -3.39 to -3.79 eV for the mono- and tri-substituted compounds, respectively, and that the second addition of electron is slightly less favorable ranging from -2.87 to -3.24 eV. The HOMO-LUMO energy gap is constant, close to 0.15 eV for the three systems independently of their number of CF_3 substituents.

DFT calculations were also carried out to get structural information on the CF_3-substituted porphyrins and to gain insights into the effect (energy, structure) of protonation and deprotonation of the inner nitrogen atoms of **P**H_2 to yield **P**H_3^+; **P**H_4^{+2} and **P**H^- and **P**$^{2-}$, respectively. The relative energies of all these species are shown in Figure ESI 36/37. Optimizations carried out on the neutral **P**H_2 molecules first confirmed that the planarity of the porphyrin ring is not affected by the number of CF_3 groups, a result which is consistent with their small size and low bulkiness. Significant distortion was however observed upon protonation and deprotonation of the inner nitrogens (Figure 8). We found that deviation from planarity is enhanced upon protonation, with an average value of 14 degrees for **4**H_3^+, **5**H_3^+ and **6**H_3^+ and 22.8 degrees for **4**H_4^{2+}, **5**H_4^{2+} and **6**H_4^{2+}. In all case, the out-of-plane distortion leads to an increase of the hydrogen…hydrogen diagonal distance from 2.15 Å to 2.50 Å (see Figure ESI 38).

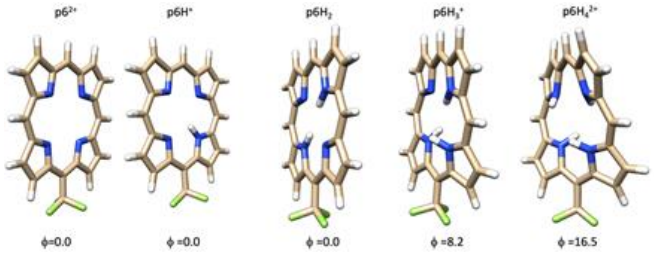

Figure 8. Optimized structures at the M06-2X/6-31G+(d,p) level of theory for the series of monosubstituted porphyrins with various protonation states.

Most importantly, these DFT data allow to compare the relative energies and stabilities of the five protonation states of each CF_3-substituted porphyrins. It also allowed provide support for the hypothesis formulated on the ground of the CV data, by demonstrating that the elimination of H_2 from the doubly reduced species **4**H_2^{2-} -> **4**$^{2-}$ + H_2 is energetically favorable by about 4.97 eV (114.5 kcal.mol^{-1}).

Conclusion

We have reported the synthesis of a series of free base porphins incorporating one, two and three CF_3 substituents, including the 5,10,15-tris(CF_3) substituted porphyrin which has never been described before. We have also carried out detailed

electrochemical and spectroscopic analyses aiming at assessing the EWG properties of the CF_3 substituents compared to the widely used C_6F_5. Our studies led us to propose an interpretation of the quite unusual electrochemical signature of these molecules featuring three successive one-electron reduction. In particular, the spectroscopic, electrochemical and spectroelectrochemical data supported by DFT calculations support the conclusion that the second irreversible reduction affords unstable dianions which are not stable at the CV time scale and evolve with elimination of dihydrogen.

Experimental Section

Synthesis and characterization

All reagents were obtained commercially unless otherwise noted. All reactions were performed in oven-dried glassware under an argon atmosphere. All solvents were dried and distilled by standard procedures. Flash column chromatography separations were achieved on silica gel (VWR 40-63 *μ*m).

^{1}H-NMR and ^{19}F-NMR spectra were recorded at room temperature on a Bruker Avance 300 or a Bruker Ascend 400 spectrometer. ^{1}H chemical shifts were referenced to residual solvent peaks. Coupling constants values (*J*) are given in hertz and chemical shifts (δ) in ppm. The abbreviations used are: s = singlet, d = doublet, t = triplet, m = multiplet and br = broad.

UV/Vis spectra were recorded on a MCS 500 or MCS 601 UV/NIR Zeiss spectrophotometer using all-quartz immersion probes (Hellma Inc.). Mass spectrometry measurements were carried out at the "Centre Commun de Spectrométrie de Masse - Lyon 1" mass spectrometry facility with a MicrOTOFQ II (Bruker) using electrospray ionization (ESI).

Electrochemistry

Acetonitrile (Acros Organics, extra-dry with molecular sieves, water < 0.005%), dimethylformamide (Sigma Aldrich, extra-dry with molecular sieves, water < 0.01%) were degassed using Freeze-Pump-Thaw procedure and were used for the spectroelectrochemical studies. The electrolyte tetra-*n*-butylammonium perchlorate (TBAP, Fluka puriss.) was purchased and used without further purification.

Cyclic voltammetry (CV) and voltammetry with rotating disc electrodes (RDE) were recorded using a SP300 Bilogic potentiostat. The analytical studies were conducted under an argon atmosphere (glove box or argon stream) in a standard one-compartment, three-electrode electrochemical cell. Tetra-*n*-butylammonium was used as supporting electrolytes (0.1 M). An automatic ohmic drop compensation procedure was systematically performed when using cyclic voltammetry. Vitreous carbon (Ø = 3 mm) working electrodes (CH Instruments) were polished with 1 mm diamond paste before each recording. Voltamperometry with a rotating disk electrode (RDE) was carried out with a radiometer (CTV101 radiometer analytical) equipment at a rotation rate of 500 rad min^{-1} using a glassy carbon RDE tip (Ø= 3 mm).

Spectroelectrochemical measurements were carried out at room temperature under an argon atmosphere (glove box or argon stream) in a standard one-compartment, three-electrode electrochemical cell with a biologic SP300 potentiostat coupled to an MCS 500 or MCS 601 UV/NIR Zeiss spectrophotometer using 1 or 10 mm all-quartz Helmma immersion probes. Electrolyses were conducted at room temperature using platinum plates (10 cm^2) working electrodes and a large piece of carbon felt as a counter-electrode isolated from the electrolytic solution through an ionic bridge. Ag/$AgNO_3$ (CH Instruments, 10^{-2} M + TBAP 10^{-1} M in CH_3CN) was used as a reference electrode.

5-Trifluoromethyldipyrromethane **(1)**

To a stirred solution of freshly distilled pyrrole (3.35 g, 50 mmol) and trifluoroacetaldehyde ethyl hemiacetal (3.60 g, 25 mmol) in dichloromethane (150 mL) was added trifluoroacetic acid (2.85, 25 mmol). The reaction was stirred for 12 h at room temperature and then treated with water (50 mL). The mixture was washed with aqueous saturated $NaHCO_3$ (50 mL) and the combined organic layers were dried over $MgSO_4$, filtered and concentrated under reduced pressure. Purification by flash chromatography on silica gel (CH_2Cl_2/heptane: 2/8) gave 1 (1.34 g, 25%) as a white solid. ^{1}H NMR ($CDCl_3$, 300 MHz): δ = 4.84 (q, 1H, J_{HF} = 8.9 Hz), 6.23 (m, 2H), 6.26 (br m, 2H), 6.76 (m, 2H), 8.06 (br s, 2H) ppm. ^{19}F NMR ($CDCl_3$, 282 MHz): δ = -68.6 (d, 3F, J_{FH} = 8.9 Hz) ppm. These values are consistent with those reported in the literature.[45]

1,9-Bis(trifluoroacetyl)-5-trifluoromethyldipyrromethane **(2)**

To a stirred solution of 1 (2.14 g, 10 mmol) in toluene (60 mL) was added trifluoroacetic anhydride (10.5 g, 50 mmol). The reaction mixture was stirred for 5 h at room temperature, treated with aqueous saturated $NaHCO_3$ (50 mL) and extracted with CH_2Cl_2 (3 × 50 mL). The combined organic layers were washed with brine (50 mL), dried over $MgSO_4$, filtered and concentrated under reduced pressure. Recrystallization in dichloromethane (30 mL) gave 2 (3.98 g, 98%) as a white solid. ^{1}H NMR (CD_3COCD_3, 300 MHz): δ = 5.63 (q, 1H, J_{HF} = 8.8 Hz), 6.64 (d, 2H, *J* = 3.9 Hz), 7.26 (m, 2H), 11.88 (br s, 2H) ppm. ^{19}F NMR (CD_3COCD_3, 282 MHz): δ = -68.7 (d, 3F, J_{FH} = 8.9 Hz), -73.3 (d, 6F, J_{FH} = 1.8 Hz) ppm. These values are consistent with those reported in the literature.[45]

1,9-Diformyl-5-trifluoromethyldipyrromethane **(3)**

To stirred and cooled (0°C) DMF (10 mL) was added phosphorus oxychloride (3.1 g, 20 mmol). The mixture was stirred for 15 min before introduction of 1 (2.03 g, 9.4 mmol) in DMF (10 mL). The reaction was stirred for 1.5 h at 0°C and then treated with aqueous saturated AcONa (10 mL). After 4 h at room temperature, the mixture was extracted with AcOEt (3 × 10 mL). The combined organic layers were washed with brine (10 mL), water (10 mL), dried over $MgSO_4$, filtered and concentrated under reduced pressure. Purification by flash chromatography on silica gel (CH_2Cl_2/AcOEt: 8/1) gave **3** (1.70 g, 67%) as a white solid. ^{1}H NMR (CD_3COCD_3, 300 MHz): δ = 5.44 (q, 1H, J_{HF} = 9.1 Hz), 6.48 (d m, 2H, J = 3.8 Hz), 7.01 (d, 2H, J = 3.8 Hz), 9.52 (s, 2H), 11.31 (br s, 2H) ppm. ^{19}F NMR (CD_3COCD_3, 282 MHz): δ = -68.9 (d, 3F, J_{FH} = 9.1 Hz) ppm. These values are consistent with those reported in the literature.[66]

Porphyrin **4**H_2

To a stirred solution of **2** (116 mg, 0.286 mmol) in THF (8.6 mL) and MeOH (2.9 mL) was added $NaBH_4$ (540.2 mg, 14.3 mmol) portion-wise over 10 min. The reaction mixture was stirred for 20 min, treated with aqueous saturated NH_4Cl (60 mL) and extracted with AcOEt (3 × 20 mL). The combined organic layers were washed with water (60 mL), dried over $MgSO_4$, filtered and concentrated under reduced pressure. The crude product was dissolved in CH_2Cl_2 (120 mL), and 1 (61 mg, 0.286 mmol) was added. The reaction mixture was degassed and heated to 35 °C before addition of $Yb(OTf)_3$ (234 mg, 0.38 mmol). The reaction mixture was stirred for 1.5 h at this temperature, and cooled to RT before sequential addition of DDQ (195 mg, 0.858 mmol) and Et_3N (0.26 mL, 1.85 mmol). The reaction mixture was filtered through a pad of silica gel (CH_2Cl_2 elution) and the solvent was removed under reduced pressure. Purification by flash chromatography on silica gel (CH_2Cl_2/pentane: 1/5) gave **4**H_2 (4.4 mg, 3%) as a brown solid. ^{1}H NMR ($CDCl_3$, 400 MHz): δ = -2.70 (s, 2H), 9.41 (d, 2H, *J* = 4.9 Hz), 9.69 (m, 2H), 9.76 (m, 4H), 11.27 (s, 1H) ppm. ^{19}F NMR ($CDCl_3$, 376 MHz): δ = -35.0 (s, 3F), -37.8 (s, 6F) ppm. ^{13}C NMR ($CDCl_3$, 100 MHz): 109.24 (s), 127.53 (q, $^1J_{C\text{-}F}$= 275 Hz), 127.87 (q, $^1J_{C\text{-}F}$= 275 Hz), 131.04 (q, $^5J_{C\text{-}F}$= 6 Hz), 132.12 (q, $^5J_{C\text{-}F}$= 6 Hz), 132.65 (q, $^5J_{C\text{-}F}$= 6 Hz), 134.12 (s), 143.97 (s),144.13 (s), 144.93 (s), 145.17 (s) ppm. The C-CF_3 peaks are expected to be quartets, and the can't be distinguished from the baseline. HRMS (ESI): calcd for $C_{23}H_{12}F_9N_4$ $[M+H]^+$ 515.0918, found 515.0903.

Porphyrin **5**H_2

To a stirred solution of **3** (77 mg, 0.286 mmol) in THF (8.6 mL) and MeOH (2.9 mL) was added $NaBH_4$ (540 mg, 14.3 mmol) portion-wise over 10 min. The reaction mixture was stirred for 20 min, treated with aqueous saturated NH_4Cl (60 mL) and extracted with AcOEt (3 × 20 mL). The combined organic layers were washed with water (60 mL), dried over $MgSO_4$, filtered and concentrated under reduced pressure. The crude product was dissolved in CH_2Cl_2 (120 mL), and **1** (61 mg, 0.286 mmol) was added. The reaction mixture was degassed and heated to 35 °C before addition of $Yb(OTf)_3$ (234 mg, 0.38 mmol). The reaction mixture was stirred for 1.5 h at this temperature, and cooled to RT before sequential addition of DDQ (195 mg, 0.858 mmol) and Et_3N (0.26 mL, 1.85 mmol). The reaction mixture was filtered through a pad of silica gel (CH_2Cl_2 elution) and the solvent was removed under reduced pressure. Purification by flash chromatography on silica gel (CH_2Cl_2/pentane: 1/5) gave **5**H_2 (10.2 mg, 8%) as a brown solid. ^{1}H NMR ($CDCl_3$, 400 MHz): δ = -2.90 (s, 2H), 9.52 (d, 4H, J = 4.8 Hz), 9.79 (m, 4H), 11.42 (s, 2H) ppm. ^{19}F NMR ($CDCl_3$, 376 MHz): δ = -38.2 (s, 6F) ppm. ^{13}C NMR ($CDCl_3$, 100 MHz): 107.31 (s), 130.37 (q, $^5J_{C\text{-}F}$= 6 Hz), 134.22 (s), 145.08 (s), 145.53 (s) ppm. The CF_3 and C-CF_3 peaks are expected to be quartets, and the can't be distinguished from the baseline. HRMS (ESI): calcd for $C_{22}H_{13}F_6N_4$ $[M+H]^+$ 447.1044, found 447.1050.

Porphyrin **6**H_2

To a stirred solution of **3** (200 mg, 0.286 mmol) in THF (8.6 mL) and MeOH (2.9 mL) was added $NaBH_4$ (540.2 mg, 14.3 mmol) portion-wise over 10 min. The reaction mixture was stirred for 20 min, treated with aqueous saturated NH_4Cl (60 mL) and extracted with AcOEt (3 × 20 mL). The combined organic layers were washed with water (60 mL), dried over $MgSO_4$, filtered and concentrated under reduced pressure. The crude product was dissolved in CH_2Cl_2 (120 mL), and 2,2'-dipyrrolylmethane (42 mg, 0.286 mmol) was added. The reaction mixture was degassed and heated to 35 °C before addition of $Yb(OTf)_3$ (234 mg, 0.38 mmol). The reaction mixture was stirred for 1.5 h at this temperature, and cooled to RT before sequential addition of DDQ (195 mg, 0.858 mmol) and Et_3N (0.26 mL, 1.85 mmol). The reaction mixture was filtered through a pad of silica gel (CH_2Cl_2 elution) and the solvent was removed under reduced pressure. Purification by flash chromatography on silica gel (CH_2Cl_2/pentane: 1/5) gave **6**H_2 (6.5 mg, 6%) as a brown solid. ^{1}H NMR ($CDCl_3$, 400 MHz): δ = -3.39 (s, 2H), 9.48 (br s, 4H), 9.54 (d, 2H, J = 4.9 Hz), 9.82 (m, 2H), 10.34 (s, 1H), 10.38 (s, 2H) ppm. ^{19}F NMR ($CDCl_3$, 376 MHz): δ = -36.7 (s, 3F) ppm. ^{13}C NMR ($CDCl_3$, 100 MHz): 106.19 (s), 106.97 (s), 128.71 (q, $^1J_{C\text{-}F}$= 275 Hz) 129.84 (q, $^5J_{C\text{-}F}$= 6 Hz), 131.73 (s), 131.89 (s), 134.01 (s),144.79 (s), 145.79 (s), 145.85 (s), 146.11 (q, $^3J_{C\text{-}F}$= 40 Hz), 146.35 (s) ppm. HRMS (ESI): calcd for $C_{21}H_{14}F_3N_4$ $[M+H]^+$ 379.1171, found 379.1163.

Acknowledgements

We thank the École Normale Supérieure de Lyon (ENSL) for financial, logistical and administrative supports. The authors gratefully acknowledge the Société Chimique de France (SCF, division NanoSciences), the GDR CNRS 2067 "Macrocycles Pyrroliques", the Région Auvergne-Rhône-Alpes and the IDEX 2020 INTERNATIONAL Joint Research Chairs (IDEX/INT/2020/19 OPE-2020-0088) for financial support.

Keywords: Porphyrins, Fluorinated Substituent, Electron-Withdrawing Group, Electrochemistry.

[1] M. Nencki, J. Zaleski *Ztschr. physiol. Ch.* **1900**, *30*, 384-485.
[2] C. J. Kingsbury, M. O. Senge *Coord. Chem. Rev.* **2021**, *431*, 213760.
[3] M. Luciano, C. Brückner *Molecules*. **2017**, *22*.
[4] J.-F. Longevial, S. Clément, J. A. Wytko, R. Ruppert, J. Weiss, S. Richeter *Chem. Eur. J.* **2018**, *24*, 15442-15460.
[5] N. Grzegorzek, A. Zieleniewska, A. Schür, C. Maichle-Mössmer, M. S. Killian, D. M. Guldi, E. T. Chernick *ChemPlusChem*. **2019**, *84*, 766-771.
[6] M. Urbani, M. Grätzel, M. K. Nazeeruddin, T. Torres *Chem. Rev.* **2014**, *114*, 12330-12396.
[7] X. Li, M. Tanasova, C. Vasileiou, B. Borhan *J. Am. Chem. Soc.* **2008**, *130*, 1885-1893.
[8] R. Zhang, J. J. Warren *ChemSusChem*. **2021**, *14*, 293-302.
[9] J. C. Biffinger, H. Sun, A. P. Nelson, S. G. DiMagno *Org. Biomol. Chem.* **2003**, *1*, 733-736.
[10] S. Saito, A. Osuka *Angew. Chem., Int. Ed. Engl.* **2011**, *50*, 4342-4373.
[11] V. V. Roznyatovskiy, C.-H. Lee, J. L. Sessler *Chem. Soc. Rev.* **2013**, *42*, 1921-1933.
[12] T. P. Wijesekera, J. E. Lyons, P. E. Ellis *Catalysis Letters*. **1996**, *36*, 69-73.
[13] R. Paolesse, S. Nardis, D. Monti, M. Stefanelli, C. Di Natale *Chem. Rev.* **2017**, *117*, 2517-2583.
[14] J. Ferrando-Soria, J. Vallejo, M. Castellano, J. Martínez-Lillo, E. Pardo, J. Cano, I. Castro, F. Lloret, R. Ruiz-García, M. Julve *Coord. Chem. Rev.* **2017**, *339*, 17-103.
[15] J. S. Lindsey *Acc. Chem. Res.* **2010**, *43*, 300-311.
[16] F. R. Kooriyaden, S. Sujatha, C. Arunkumar *Polyhedron*. **2015**, *97*, 66-74.
[17] C. Arunkumar, F. R. Kooriyaden, S. Sujatha.
[18] C. H. Devillers, S. Hebié, D. Lucas, H. Cattey, S. Clément, S. Richeter *J. Org. Chem.* **2014**, *79*, 6424-6434.
[19] A. Giraudeau, H. J. Callot, J. Jordan, I. Ezhar, M. Gross *J. Am. Chem. Soc.* **1979**, *101*, 3857-3862.
[20] T. Goslinski, J. Piskorz *J. Photochem. Photobiol. C*. **2011**, *12*, 304-321.
[21] K. L. Kirk *J. Fluor. Chem.* **2006**, *127*, 1013-1029.
[22] V. M. Muzalevskiy, A. V. Shastin, E. S. Balenkova, G. Haufe, V. G. Nenajdenko *Synthesis*. **2009**, *23*, 3905-3929
[23] T. Yoshimura, H. Toi, S. Inaba, H. Ogoshi *Inorg. Chem.* **1991**, *30*, 4315-4321.
[24] J. Leroy, A. Bondon *Eur. J. Org. Chem.* **2008**, *2008*, 417-433.
[25] X.-G. Chen, C. Liu, D.-M. Shen, Q.-Y. Chen *Synthesis*. **2009**, *2009*, 3860-3868.
[26] C. Liu, D.-M. Shen, Q.-Y. Chen *J. Am. Chem. Soc.* **2007**, *129*, 5814-5815.
[27] Y. Terazono, D. Dolphin *J. Org. Chem.* **2003**, *68*, 1892-1900.
[28] C. Liu, Q.-Y. Chen *Eur. J. Org. Chem.* **2005**, *2005*, 3680-3686.
[29] R. Goldschmidt, I. Goldberg, Y. Balazs, Z. Gross *J. Porphyr. Phtalocyanines*. **2006**, *10*, 76-86.
[30] X. Zhan, P. Yadav, Y. Diskin-Posner, N. Fridman, M. Sundararajan, Z. Ullah, Q.-C. Chen, L. J. W. Shimon, A. Mahammed, D. G. Churchill, M.-H. Baik, Z. Gross *Dalton Trans.* **2019**, *48*, 12279-12286.
[31] K. Sudhakar, A. Mahammed, N. Fridman, Z. Gross *Dalton Trans.* **2019**, *48*, 4798-4810.
[32] S. Shimizu, N. Aratani, A. Osuka *Chem. Eur. J.* **2006**, *12*, 4909-4918.
[33] M. Suzuki, S. Ishii, T. Hoshino, S. Neya *Chem. Lett.* **2014**, *43*, 1563-1565.
[34] D. Lahaye, K. Muthukumaran, C. H. Hung, D. Gryko, J. S. Rebouças, I. Spasojević, I. Batinić-Haberle, J. S. Lindsey *Bioorg Med Chem*. **2007**, *15*, 7066-7086.
[35] T. P. Wijesekera *Can. J. Chem.* **1996**, *74*, 1868-1871.
[36] N. Nishino, R. W. Wagner, J. S. Lindsey *J. Org. Chem.* **1996**, *61*, 7534-7544.
[37] T. Wijesekera, J. E. Lyons, P. E. Ellis in Method for oxidizing alkanes using novel porphyrins synthesized from dipyrromethanes and aldehydes, Vol. 5,990,363 (Ed.^Eds.: Editor), City, **1999**.
[38] T. Wijesekera, J. E. Lyons, P. E. Ellis, Jr., M. V. Bhinde in Preparation of porphyrins and metal complexes thereof having haloalkyl side chains as catalysts for oxidation of alkanes and for the decomposition of hydroperoxides, Vol. (Ed.^Eds.: Editor), Sun Company, Inc. (R&M), City, **1997**.
[39] A. Nemes, E. Mérész, I. Jalsovszky, D. Szabó, Z. Böcskei, J. Rábai *J. Fluor. Chem.* **2017**, *203*, 75-80.
[40] J. G. Goll, K. T. Moore, A. Ghosh, M. J. Therien *J. Am. Chem. Soc.* **1996**, *118*, 8344-8354.
[41] S. A. Syrbu, S. G. Pukhovskaya, D. The Nam, Y. B. Ivanova, M. I. Razumovd *Macroheterocycles*. **2019**, *12*, 135-142.
[42] J. C. Grancho, M. M. Pereira, G. Miguel Mda, G. A. Rocha, H. D. Burrows *Photochem Photobiol*. **2002**, *75*, 249-256.
[43] S. G. Pukhovskaya, Y. B. Ivanova, D. T. Nam, A. S. Semeikin, S. A. Syrbu, N. Z. Mamardashvili *Russ. J. Gen. Chem.* **2019**, *89*, 586–596.
[44] S. M. Landge, D. A. Borkin, B. Török *Tetrahedron Lett.* **2007**, *48*, 6372-6376.
[45] W. Dmowski, K. Piasecka-Maciejewska, Z. Urbanczyk-Lipkowska *ChemInform*. **2003**, *34*.
[46] P.-G. Julliard, S. Pascal, O. Siri, D. Cortés-Arriagada, L. Sanhueza, G. Canard *Comptes Rendus Chimie*. **2021**, *24*, 1-19.
[47] P. D. Rao, S. Dhanalekshmi, B. J. Littler, J. S. Lindsey *J. Org. Chem.* **2000**, *65*, 7323-7344.
[48] C. Brückner, J. J. Posakony, C. K. Johnson, R. W. Boyle, B. R. James, D. Dolphin *J. Porphyr. Phtalocyanines*. **1998**, *02*, 455-465.

[49] J. R. Frost, S. M. Huber, S. Breitenlechner, C. Bannwarth, T. Bach *Angew. Chem., Int. Ed. Engl.* **2015**, *54*, 691-695.
[50] D. Lahaye, K. Muthukumaran, C.-H. Hung, D. Gryko, J. S. Rebouças, I. Spasojević, I. Batinić-Haberle, J. S. Lindsey *Bioorg. Med. Chem.* **2007**, *15*, 7066-7086.
[51] K. M. Kadish, M. M. Morrison *J. Am. Chem. Soc.* **1976**, *98*, 3326-3328.
[52] V. L. Balke, F. A. Walker, J. T. West *J. Am. Chem. Soc.* **1985**, *107*, 1226-1233.
[53] Y. Cui, L. Zeng, Y. Fang, J. Zhu, H.-J. Xu, N. Desbois, C. P. Gros, K. M. Kadish *ChemElectroChem*. **2016**, *3*, 110-121.
[54] C. M. A. Brett, A. M. C. F. O. Brett *J. Electroanal. Chem.* **1988**, *255*, 199-213.
[55] K. M. Kadish, G. Royal, E. Van Caemelbecke, L. Gueletti in *The Porphyrin Handbook, Vol. 9, Chap 59* (Ed. K. S. K. M. Kadish, R. Guilard), Academic Press, **2000**, pp.1-220.
[56] K. M. Kadish, E. Van Caemelbecke *J. Solid State Electrochem.* **2003**, *7*, 254-258.
[57] C. Bucher, C. H. Devillers, J.-C. Moutet, G. Royal, E. Saint-Aman *Chem. Commun.* **2003**, 888-889.
[58] C. Bucher, C. H. Devillers, J.-C. Moutet, G. Royal, E. Saint-Aman *New J. Chem.* **2004**, *28*, 1584-1589.
[59] D. W. Clack, N. S. Hush *J. Am. Chem. Soc.* **1965**, *87*, 4238-4242.
[60] X. Ke, P. Yadav, L. Cong, R. Kumar, M. Sankar, K. M. Kadish *Inorg. Chem.* **2017**, *56*, 8527-8537.
[61] N. Chaudhri, L. Cong, A. S. Bulbul, N. Grover, W. R. Osterloh, Y. Fang, M. Sankar, K. M. Kadish *Inorg. Chem.* **2020**, *59*, 1481-1495.
[62] W. R. Osterloh, S. Kumar, N. Chaudhri, Y. Fang, M. Sankar, K. M. Kadish *Inorg. Chem.* **2020**, *59*, 16737-16746.
[63] C. Amatore, G. Capobianco, G. Farnia, G. Sandona, J. M. Saveant, M. G. Severin, E. Vianello *J. Am. Chem. Soc.* **1985**, *107*, 1815-1824.
[64] C. Costentin, M. Robert, J.-M. Savéant *Chem. Rev.* **2010**, *110*, PR1-PR40.
[65] Y. Fang, P. Bhyrappa, Z. Ou, K. M. Kadish *Chem. Eur. J.* **2014**, *20*, 524-532.
[66] J. Heinze in *Aliphatic and Aromatic Hydrocarbons: Reduction, Vol.* (Eds.: O. Hammerich, B. Speiser), CRC Press, Boca Raton, **2015**, pp.861-889.
[67] D. E. Bartak, M. D. Hawley *J. Am. Chem. Soc.* **1972**, *94*, 640-642.
[68] K. J. Borhani, M. Dale Hawley *J. Electroanal. Chem.* **1979**, *101*, 407-417.